Pergamon

Int. J. Multiphase Flow Vol. 22, No. 3, pp. 575–591, 1996

0301-9322(95)00080-1
0301-9322/96 $15.00 + 0.00

AN EXPERIMENTAL AND NUMERICAL STUDY OF FLOW PATTERNS IN A CIRCULATING FLUIDIZED BED REACTOR

A. SAMUELSBERG and B. H. HJERTAGER

Department of Process Technology (IPT) at Telemark Institute of Technology (HiT-TF) and Telemark Technological R&D Centre (Tel-Tek), Kjølnes Ring, N-3914 Porsgrunn, Norway

(Received 3 January 1995; in revised form 13 November 1995)

Abstract—This paper presents an experimental and a numerical study on radial profiles of axial particle velocity component in a cold flow laboratory scale circulating fluidized bed reactor. Laser Doppler anemometry (LDA) has been used to measure mean and root mean square (RMS) particle velocities for three different superficial gas velocities. A two dimensional two phase flow model with a turbulent kinetic energy equation based on kinetic theory of granular flow is verified against the experimental data. The model is based on a Eulerian description of the two phases, gas and particles. The time averaged predictions are in good accordance with the experiments. The model predicts a core annulus flow, similar to that found experimentally. The predicted maximum velocity in the core agrees well with the measurements, but the model overpredicts the downflow velocity near the wall. Calculated RMS velocity profiles are in good agreement with the experimental data. Copyright © 1996 Elsevier Science Ltd.

Key Words: LDA, CFD, multi phase modelling, circulating fluidized bed, numerical simulation, kinetic theory of granular flow

1. INTRODUCTION

1.1. The problem

Circulating fluidized bed reactors (CFB) are widely used in industry. Major applications are fluid catalytic cracker (FCC) risers and CFB combustors. Despite the huge economical investments needed in building new or upgrading existing CFBs, very little is known about the fluid dynamics behaviour of CFBs. No analytical tools are available which can describe the influences of complex geometries, multiple gas-inlets, chemical reaction, internal reflux and heat transfer on the flow pattern. Several models for describing the hydrodynamics of CFBs has been published during the last 30 years. These models can be divided into three broad groups (Harris & Davidson 1993). The first group involves models that predict the axial distribution of the solid phase, but are not able to predict the radial variation of solids. The second group includes models that divide the flow into two or more distinct regions. The third group comprises models which are based on numerical modelling of the conservation equations for mass, momentum and energy for both phases. Such models give the axial and radial variation of the velocity components, enthalpy and volume fraction of the phases involved.

1.2. Previous work

Hydrodynamic modelling of fluidized bed reactors, based on first principles, started some 25–30 years ago. Gidaspow (1993) has reviewed the models developed until 1985. At that time the models were able to simulate gas bubble formation, propagation and bursting in a fluidized bed using an inviscid two fluid model. Tsuo & Gidaspow (1990) extended the model with an apparent viscosity, which made it possible to predict radial and axial variations of volume fractions and velocities for both phases in a circulating fluidized bed. Ma & Ahmadi (1990), Sinclair & Jackson (1989), Ding & Gidaspow (1990), and Gidaspow (1992) developed a turbulence model for the particulate phase which made it possible to calculate the shear viscosity directly in the solid phase, based on the random motion of particles. Even though the proposed models are able to predict the particle fluctuations no comparisons of measured and predicted fluctuations have appeared in literature.

1.3. Objectives

This paper presents an isothermal two-phase multi dimensional gas particle flow model based on a kinetic theory description given by Gidaspow (1992). This model will be verified against experimental data from a laboratory scale circulating fluidized bed reactor. Particular emphasis will be given to the investigation of the large and small scale velocity fluctuations in the particulate phase.

2. EXPERIMENTAL APPARATUS AND METHODS

The laboratory scale reactor which is made of plexiglass, is 1 m high with an internal diameter of $d = 0.032$ m. The separation unit is a cyclone made of glass. The particles are separated from the gas and re-injected back to the reactor with the supply of secondary air, positioned 0.05 m above the gas distributor. The initial bed height of the catalysts is 0.05 m. The distributor is a Duran filterplate, type 112 004-2 with diameter 0.04 m with a thickness of 0.004 m. The porosity of the distributor is 0.36. A sketch of the reactor is showed in figure 1.

The LDA, delivered by DANTEC, is used to measure the radial profiles of the local axial velocity component and the root mean square (RMS) velocity of the particles, at heights 0.16, 0.32 and 0.48 m above the gas distributor.

The LDA is applied in forward scatter mode using a transmitting lens of 600 mm focal length a beam separation of 38 mm and a receiving lens of 310 mm focal length with an effective scattering angle of 136°. The laser source is a 2-W Spectra-physics Stabilite 2016 Argon–Ion laser operated at a wavelength of 514.5 nm. One of the beams had an optical frequency shift of 40 MHz. An IBM compatible PC/AT computer is used on-line to sample and process the data. The radial spacing between the measurements is 2 mm, i.e. eight points cover the radial distance. The local particle

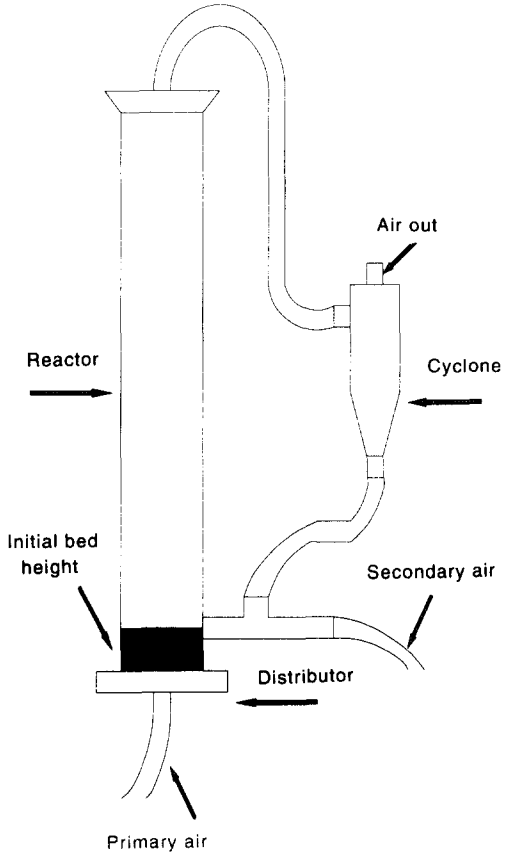

Figure 1. Laboratory scale reactor with recirculation.

velocity and RMS velocity are the means of 1000 accepted samples in each measured point. The density of the FCC particles is 1600 kg/m^3 with a Sauter mean diameter of 60 μm, the smallest diameter is about 20 μm and the largest diameter is about 150 μm. The superficial gas velocity used in the experiments are 0.36, 0.71 and 1.42 m/s at ambient temperature. The secondary air is held constant at 0.05 m/s to prevent the particles to build up in the standpipe.

3. NUMERICAL MODELLING

3.1. Fluid dynamic model

We are using the two fluid model for our analyses. This means that the laws of conservation of mass and momentum are satisfied by each phase individually. The following dependent variables are solved for each phase separately: ϵ (volume fractions), U and V (velocity components) and p (pressure). In addition, a turbulent kinetic energy equation, based on kinetic theory of dense gases is solved for the solid phase which gives the granular temperature.

3.2. Kinetic model for the solid phase

For the particulate phase, a comprehensive model, which is based on kinetic theory of dense gases, is adopted. Lun *et al.* (1984) and Jenkins & Savage (1983) were first to start this work. Ding & Gidaspow (1990) continued their work and made the model valid for dense particulate flow. Gidaspow (1992) extended this model further and made the model valid for dilute particle flow.

The constitutive equations come from interactions of the fluctuating and mean motions of the particles. These interactions generate stresses and give rise to an effective viscosity for the solid phase which relates the random fluctuating motion to the mean motion of the particles. In order to predict the random fluctuations, the equations for conservation of mass, momentum and fluctuating energy are derived for the particulate phase. The thermal temperature in kinetic theory of gases is here replaced with a granular temperature, for which a transport equation is derived. The solid viscosity and thereby the solid stresses depend on this granular temperature.

The governing equations written in Cartesian tensor notation, may then be formulated as (Gidaspow 1992):

Mass balances.

Gas phase:

$$\frac{\partial(\epsilon\rho)_g}{\partial t} + \frac{\partial(\epsilon\rho U_i)_g}{\partial x_i} = 0. \qquad [1]$$

Solid phase:

$$\frac{\partial(\epsilon\rho)_s}{\partial t} + \frac{\partial(\epsilon\rho U_i)_s}{\partial x_i} = 0, \qquad [2]$$

where ϵ is volume fraction, ρ is the density, t is time, x_i is coordinate direction in i-direction, U_i and U_j are the i and j-component of velocity for gas and solid. Finally, the subscripts g denote gas phase and s the solid phase. These equations are valid with no mass transfer between the phases.

Momentum balances.

Gas phase:

$$\frac{\partial(\epsilon\rho U_j)_g}{\partial t} + \frac{\partial(\epsilon\rho U_i U_j)_g}{\partial x_i} = -\epsilon_g \frac{\partial P}{\partial x_j} + \epsilon_g \rho_g g_j + \frac{\partial \tau_{ij}}{\partial x_i} + \beta_f (U_{j,s} - U_{j,g}). \qquad [3]$$

Here g_j is the j-direction component of gravity, p is the pressure, τ is stress tensor in the gas phase and β is the two phase drag coefficient. The shear stress is related to the gradients of velocity components as:

$$\tau_{i,j} = \mu_g \left[\left(\frac{\partial U_j}{\partial x_i} + \frac{\partial U_i}{\partial x_j} \right) - \tfrac{2}{3}\delta_{i,j} \frac{\partial U_k}{\partial x_k} \right], \qquad [4]$$

where μ is the shear viscosity and δ_{ij} is the Kroenecker delta. The turbulent viscosity in the gas phase is modelled with use of a Sub Grid Scale (SGS) model, first used by Deardorff (1971). The

local Reynold's stresses, which arises from averaging over the finite difference cell are simulated by the SGS model.

This SGS eddy coefficient is limited by the averaging domain, which in two dimensions is considered to be the grid volume $\Delta x \Delta y$.

The SGS model for turbulent viscosity can be written:

$$\mu_g = \rho_g (c_t \Delta)^2 (\tau_{i,j} \cdot \tau_{i,j}) \qquad [5]$$

$$\text{with } c_t = 0.1 \text{ and } \Delta = \sqrt{\Delta x \cdot \Delta y}.$$

Solid phase:

$$\frac{\partial(\epsilon\rho \mathrm{U}_j)_s}{\partial t} + \frac{\partial(\epsilon\rho U_i U_j)_s}{\partial x_i} = -\epsilon_s \frac{\partial P}{\partial x_j} + \epsilon_s \rho_s g_j + \frac{\partial}{\partial x_i} \Pi_{i,j} + \beta_f (U_{j,g} - U_{j,s}). \qquad [6]$$

Here Π is the stress tensor in the solid phase. The total shear stress in the solid phase is the sum of a collisional part and a kinetic part and may be formulated as:

$$\Pi_{i,j} = -P_s \delta_{ij} + \xi_s \delta_{ij} \frac{\partial U_k}{\partial x_k} + \mu_s \left[\left(\frac{\partial U_j}{\partial x_i} + \frac{\partial U_i}{\partial x_j} \right) - \tfrac{2}{3} \delta_{ij} \frac{\partial U_k}{\partial x_k} \right], \qquad [7]$$

where ξ is the solid bulk viscosity. The solid phase pressure, P_s, which includes both kinetic and collisional pressures, is determined from an equation of state similar to the van der Waals equation of state for gases Chapman & Cowling (1970)

$$P_s = \epsilon_s \rho_s [1 + 2(1 + e)\epsilon_s g_0] \Theta. \qquad [8]$$

Here, e is the coefficient of restitution and g_0 is the radial distribution function (Lun *et al.* 1984) which is equal to one when the particles are loosely packed and becomes infinite when they are so closely packed that motion is impossible. Θ is the granular temperature related to the kinetic turbulent energy of the particle motion.

A form of the radial distribution function adopted by Ding & Gidaspow (1990) is

$$g_0 = \left[1 - \left(\frac{\epsilon_s}{\epsilon_{s,\max}} \right)^{1/3} \right]^{-1}, \qquad [9]$$

where $\epsilon_{s,\max}$ is the maximum solid volume fraction of a random packing. In the following computations, $\epsilon_{s,\max}$ equal to 0.65 is used.

Solid phase bulk viscosity due to particle collisions can be written as:

$$\xi_s = \tfrac{4}{3} \epsilon_s^2 \rho_s d_p g_0 (1 + e) \sqrt{\frac{\Theta}{\pi}}. \qquad [10]$$

Here d_p is the particle diameter.

The solid phase shear viscosity for dense and dilute flow is given by:

$$\mu_s = \frac{2\mu_{s,\mathrm{dil}}}{(1 + e)g_0} [1 + \tfrac{4}{5}(1 + e) g_0 \epsilon_s]^2 + \tfrac{4}{5} \epsilon_s^2 \rho_s d_p g_0 (1 + e) \sqrt{\frac{\Theta}{\pi}}$$

$$\mu_{s,\mathrm{dil}} = \tfrac{5}{96} \rho_s d_p \sqrt{\pi \Theta}. \qquad [11]$$

The viscosity is seen to be a product of the mean free path times an oscillation velocity times a density.

Gas solid drag coefficient. For $\epsilon_g \leqslant 0.8$ (based on the Ergun equation)

$$\beta = 150 \frac{\epsilon_s^2 \mu_g}{\epsilon_g (d_p \phi_s)^2} + 1.75 \frac{\epsilon_s \rho_g |\mathbf{U}_g - \mathbf{U}_s|}{d_p \phi_s}. \qquad [12]$$

For $\epsilon_g > 0.8$ (based on empirical correlation)

$$\beta = \tfrac{3}{4} C_d \frac{|\mathbf{U}_g - \mathbf{U}_s| \rho_g \epsilon_s}{d_p \phi_s} \alpha \epsilon_g^{-2.65}, \qquad [13]$$

where Φ_s is a measure of the sphericity,

$$C_d = \frac{24}{\mathrm{Re}}(1 + 0.15\mathrm{Re}^{0.687}) \text{ for } \mathrm{Re} \leqslant 1000$$

$$C_d = 0.44 \text{ for } \mathrm{Re} > 1000$$

$$\mathrm{Re} = \frac{|\mathbf{U}_g - \mathbf{U}_s|\epsilon_g \rho_g d_p}{\mu_{l,g}} \quad [14]$$

Here C_d is the drag coefficient and Re is the Reynolds number.

Granular temperature or turbulent kinetic energy.

$$\frac{3}{2}\left[\frac{\partial}{\partial t}(\epsilon\rho\Theta)_s + \frac{\partial}{\partial x_i}(\epsilon\rho U_i\Theta)_s\right] = \Pi_{i,j}\frac{\partial U_{j,s}}{\partial x_i} - \frac{\partial}{\partial x_i}\left[\Gamma_\Theta \frac{\partial \Theta}{\partial x_i}\right] - \gamma. \quad [15]$$

Here Γ is the transport coefficient or conductivity and γ is the collisional energy dissipation expressed as:

$$\gamma = 3(1 - e^2)\epsilon_s^2 \rho_s g_0 \Theta\left[\frac{4}{d_p}\sqrt{\frac{\Theta}{\pi}} - \frac{\partial U_{k,s}}{\partial x_k}\right]. \quad [16]$$

For a restitution coefficient of one, that is perfectly elastic collision, no energy is lost in the collision and γ equals zero.

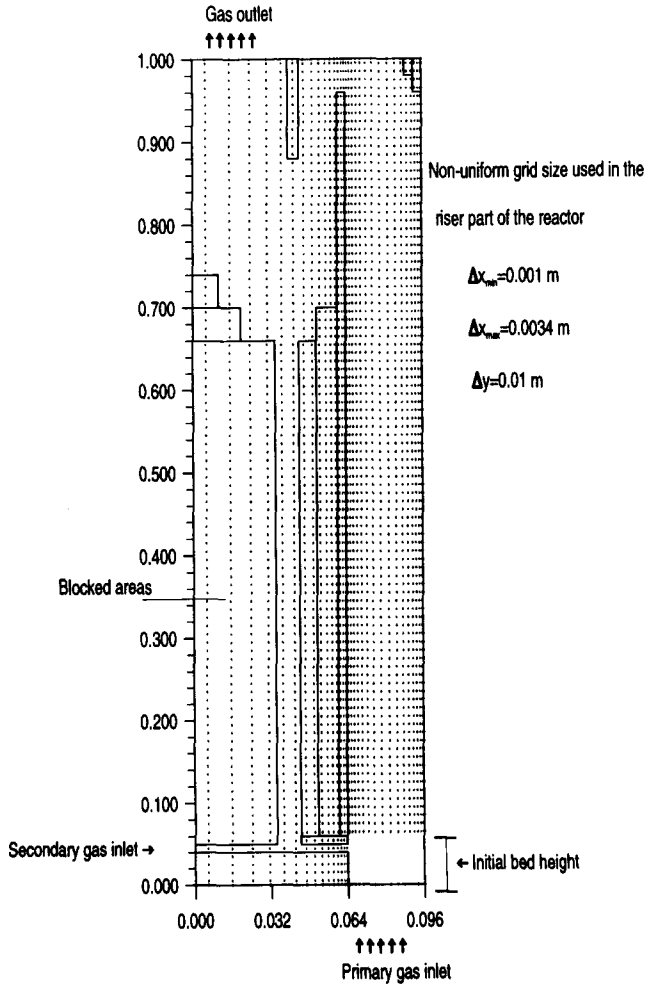

Figure 2. The calculation area with expanded grid.

Conductivity of fluctuating energy.

$$\Gamma_\Theta = \frac{2\Gamma_{\Theta,\mathrm{dil}}}{(1+e)g_0}[1+\tfrac{6}{5}(1+e)g_0\epsilon_s]^2 + 2\epsilon_s^2\rho_s d_p g_0(1+e)\sqrt{\frac{\Theta}{\pi}}$$

$$\Gamma_{\Theta,\mathrm{dil}} = \tfrac{75}{384}\rho_s d_p\sqrt{\pi\Theta}. \qquad [17]$$

4. SOLUTION PROCEDURE

The governing set of partial differential equations are solved by the numerical solution procedure of Spalding (1985). The transport equations are discretized by a finite volume method. The

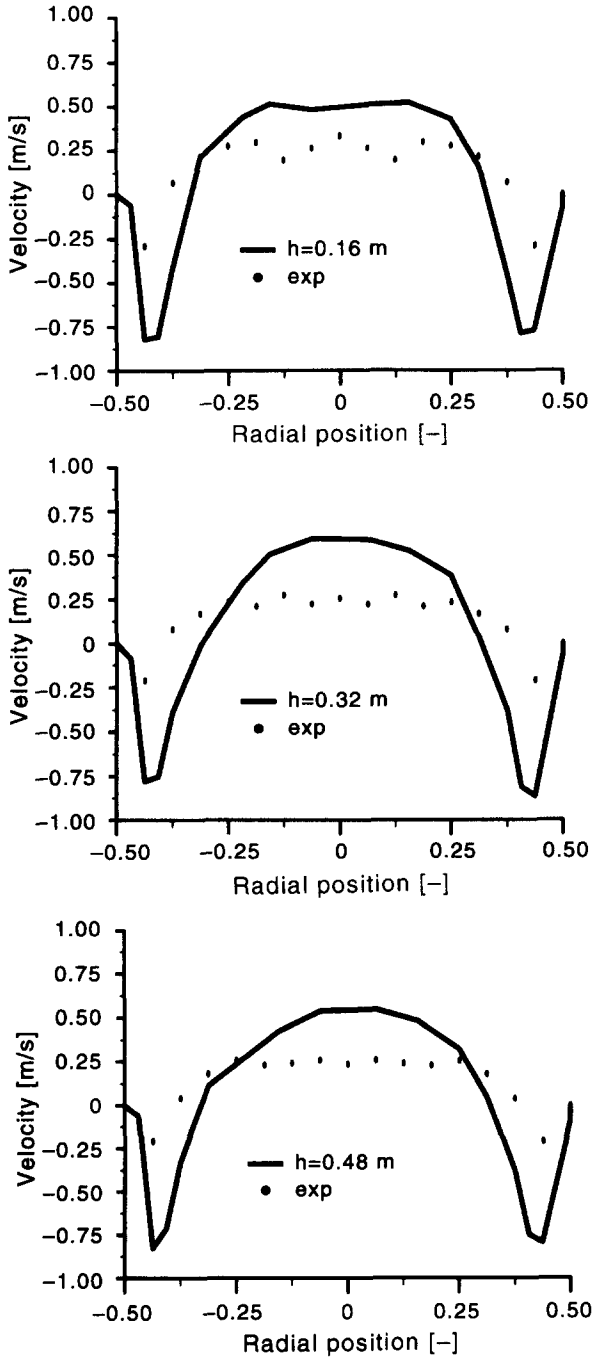

Figure 3. Experimental and simulated particle velocity. $V_{g,\mathrm{sup}} = 0.36$ m/s.

computational domain is therefore divided into a finite number of non-overlapping control volumes, such that there is one control volume surrounding each grid point. Scalar variables like pressure, void fractions, turbulent quantities and densities are stored at the grid points. For the velocity components a staggered grid is used. The velocities are located on the faces of the control volumes. The transport equations are integrated over each control volume in space in a manner that the integral conservation is satisfied over the calculation domain and over a time interval.

The integration is performed using upwind differencing in space and implicit differencing in time. The time step is limited by the Courant criteria.

For the volume-fraction, velocity and turbulent kinetic energy equation, a point iteration method is used. Because of the strong coupling between the phases in the momentum equations, the partial

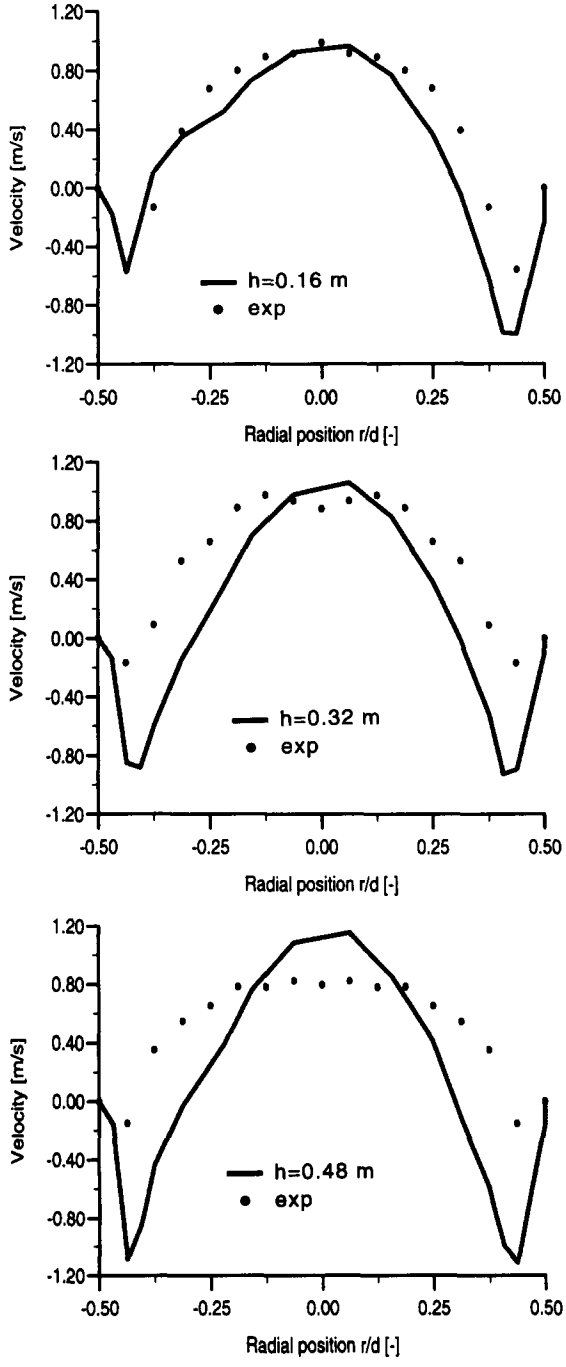

Figure 4. Experimental and simulated particle velocity. $V_{g,sup} = 0.71$ m/s.

elimination algorithm (PEA) is used to decouple the drag force in the velocity equation. The coupling between pressure and velocity is handled by the inter-phase slip algorithm (IPSA).

5. EXPERIMENTAL AND NUMERICAL RESULTS

5.1. Initial and boundary conditions

The reactor was represented in a Cartesian grid with expansion of the grid in the radial direction. 32 × 102 grid nodes were used in the radial and axial directions, respectively. This gave a total of 16 grid nodes across the riser. The expanded grid is shown in figure 2. The asymmetric outlet was

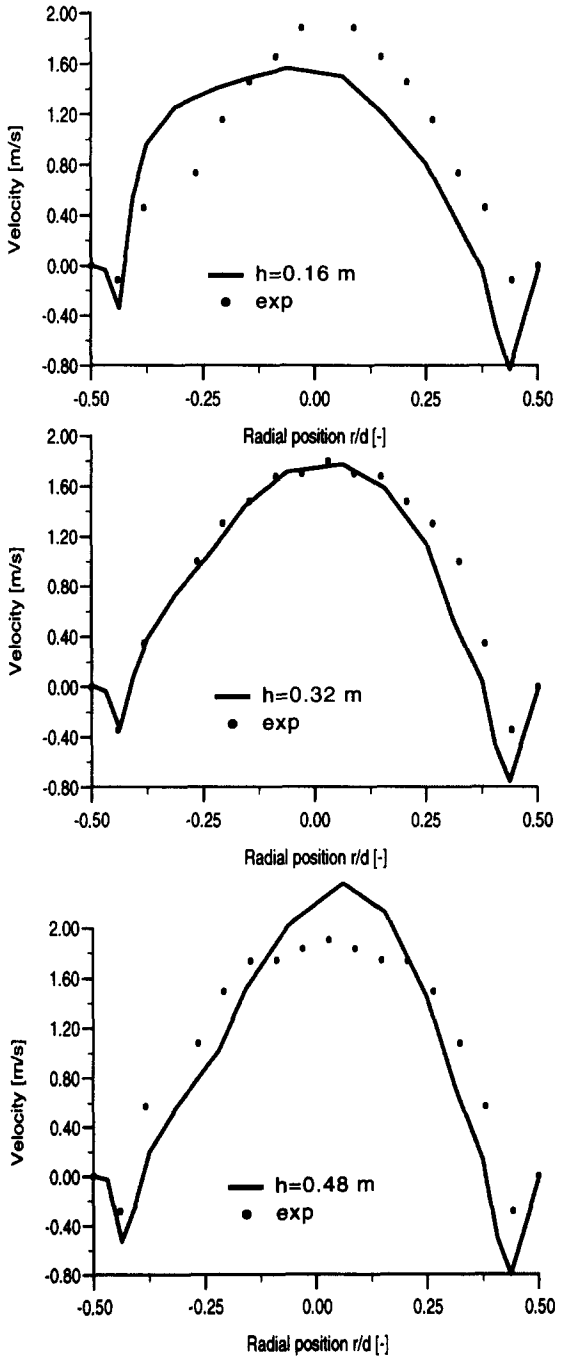

Figure 5. Experimental and simulated particle velocity. $V_{g,sup} = 1.42$ m/s.

chosen due to limited grid resolution. However, the outlet assumption does not significantly influence the predictions since the particle downflow is mainly governed by gravity and transverse momentum exchange, not so much by axial momentum exchange. The grid distribution used was chosen based on previous grid dependence tests performed in a similar riser. Initially the reactor is filled with a 0.05 m high bed with 60 μm diameter particles and density 1600 kg/m^3. One dimensional plug flow is assumed at the primary gas inlet boundary. The secondary gas inlet is held at a constant velocity of 0.05 m/s. At the outlet, a continuation condition for the gas phase is used. No particles are allowed to leave the reactor. At the wall boundaries, a no-slip condition for the gas phase and a slip condition for the solid phase are imposed. The turbulent kinetic energy

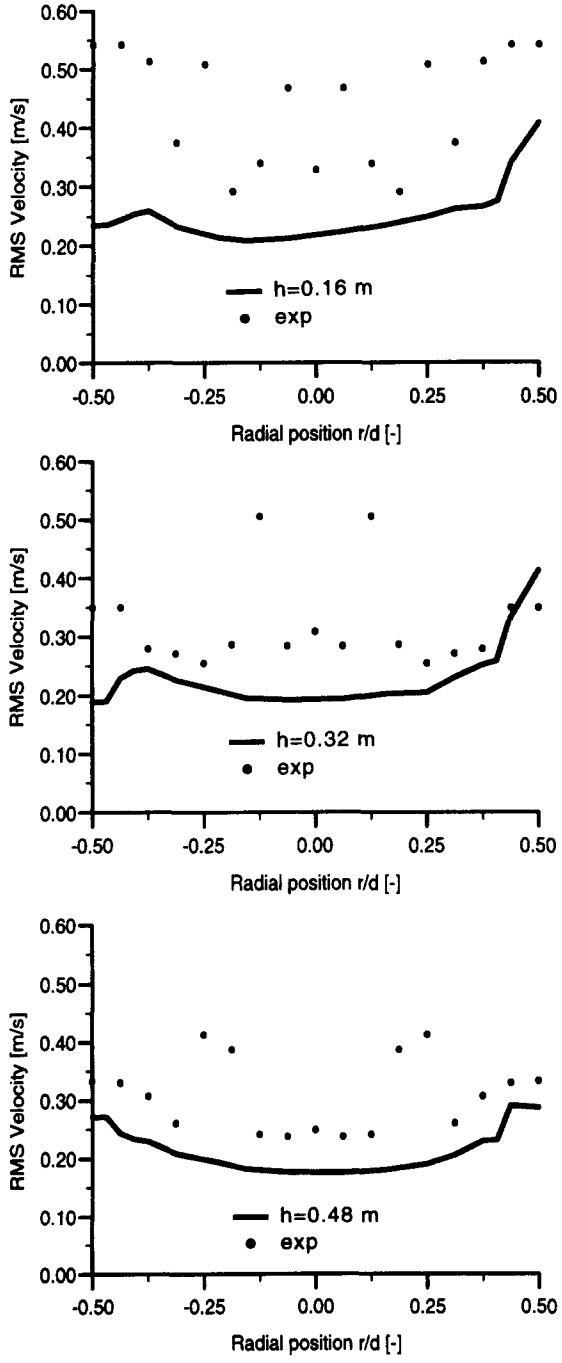

Figure 6. Experimental and simulated particle RMS velocity. $V_{g,sup} = 0.36$ m/s.

flux at the wall is zero, because the restitution coefficient between the wall and the particles is unknown. A wall law will then only introduce an unknown parameter. The computations are compared against three experimental isothermal gas-particle flow situations. The simulations ran for 12 s of real simulation time for the gas superficial velocity $V_{g,sup} = 0.36$ m/s and 10 s for the other superficial gas velocities. In order to get a reasonable time average to compare against the experimental data, a time average was obtained from the last two seconds of the simulations. A restitution coefficient of 0.995, was used in all simulations.

5.2. *Velocity profiles*

As illustrated in figures 3–5, the predicted particle velocities have the same general trend as

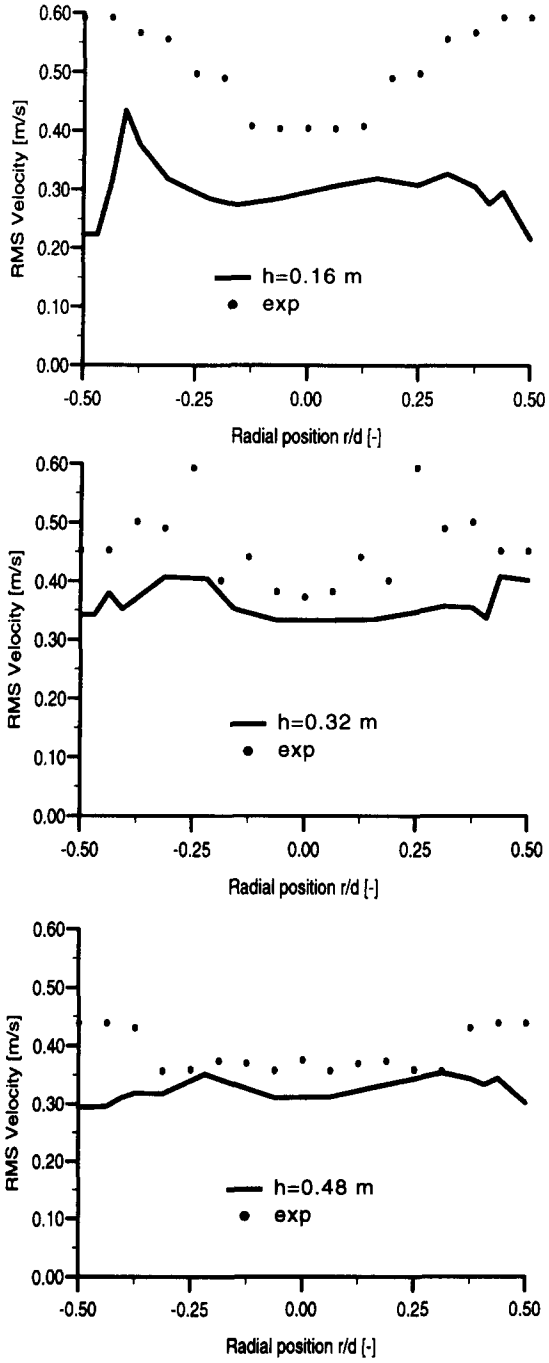

Figure 7. Experimental and simulated particle RMS velocity. $V_{g,sup} = 0.71$ m/s.

measured. The particles move upwards in the core and downwards near the walls. A behaviour which is typical for core-annulus flow. In figure 3, for the lowest gas superficial velocity $V_{g,sup} = 0.36$ m/s, the particle velocity has the same even and flat distribution, even if the predicted core velocity is too high. In the annulus however, the simulations give a somewhat higher velocity near the wall than measured. Predicted downflow velocity is seen to have the same magnitude at all heights.

Since the velocity in the core is overpredicted, the core diameter is smaller than the measured. From the velocity profiles the flow seems to be fully developed.

For gas superficial velocity $V_{g,sup} = 0.71$ m/s, figure 4 shows how the velocity profiles compares

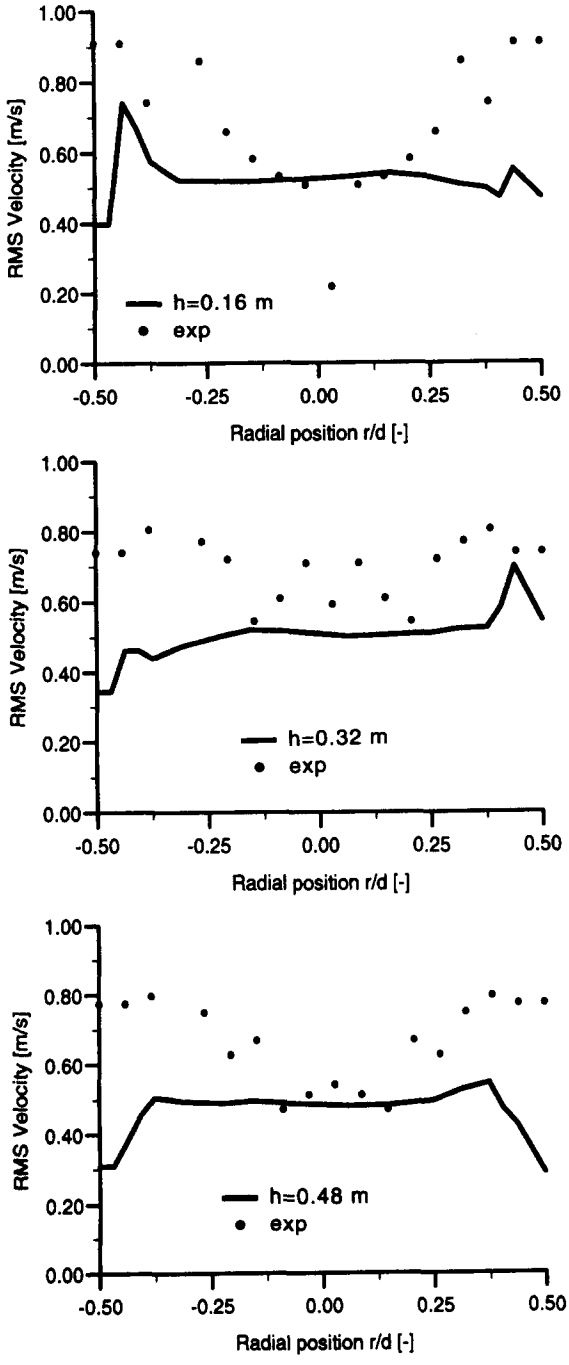

Figure 8. Experimental and simulated particle RMS velocity. $V_{g,sup} = 1.42$ m/s.

well with the experimental results in the core of the reactor at all heights. The core annulus flow in the simulations gives the general trend, but a little too high central velocity at the highest level. The downflow near the wall is overpredicted at all heights. The simulations are not quite symmetrical at the two lowest heights. This may be due to the asymmetrical backflow of particles. There is a slight acceleration of the particles throughout the riser, hence the flow is not fully developed.

When the gas superficial velocity is $V_{g,sup} = 1.42$ m/s, the simulations are in good agreement with the experiments. The velocity profile in the core is a little too low at 0.16 m and a little too high at 0.48 m. The particles are accelerated upwards at all heights, a finding also supported by the experiments. The velocity gradients are getting steeper when moving upwards in the riser. The annulus is well predicted at the left side of the riser, but at the right side the down flow is overpredicted. The overprediction of the downflow velocities in figures 3–5 may be due to the fact that electrostatic forces present in the experiments were not incorporated in the model.

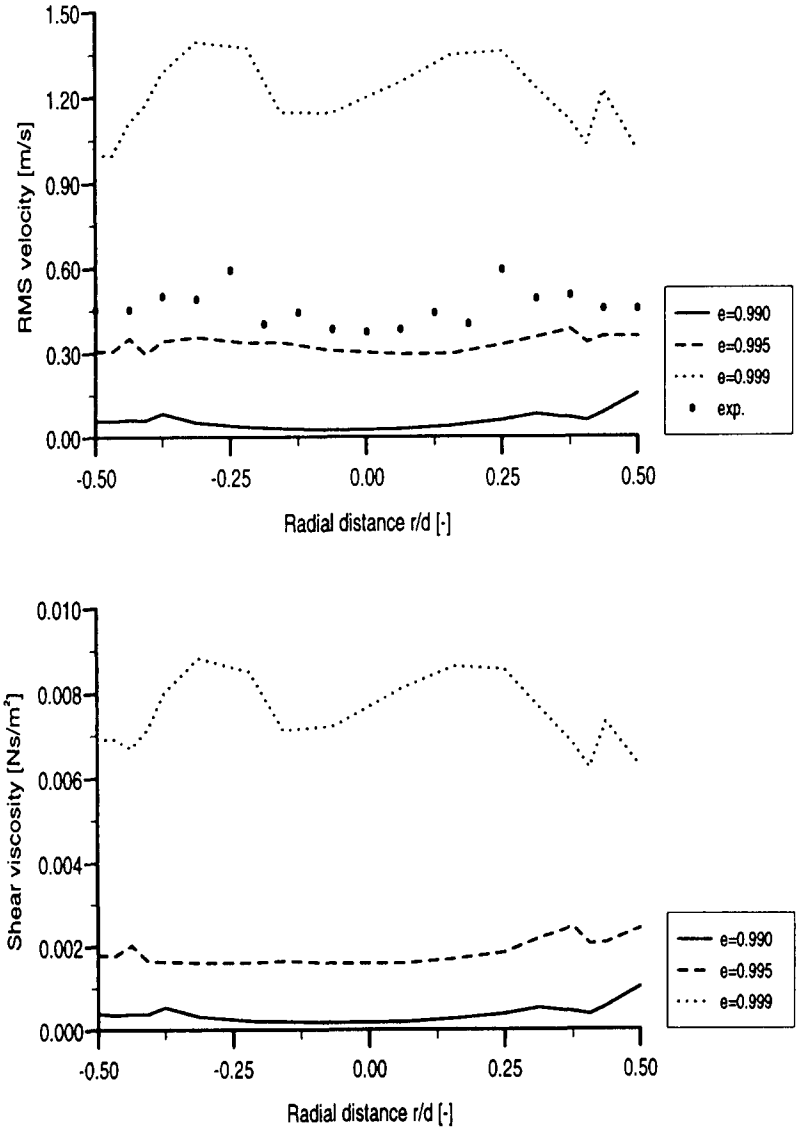

Figure 9. Effect of restitution coefficient on granular temperature and shear viscosity.

5.3. *RMS velocity profiles*

The RMS velocity is derived from the granular temperature through the relation $V_{RMS} = (3 \times \Theta)^{1/2}$. From the experiments the RMS velocity is found from the relation:

$$V_{RMS} = \sqrt{\frac{1}{n-1}\sum_{j=1}^{n}(V_j - \bar{V})^2}$$

$$\text{where } \bar{V} = \frac{1}{n}\sum_{j=1}^{n} V_j.$$

A comparison between the simulated RMS velocity and the measured RMS velocity is therefore possible. Figures 6–8 show the experimental and simulated RMS velocity for superficial gas velocity of 0.36, 0.71 and 1.42 m/s, respectively. The general trend in the simulations is in relatively good agreement with the experimental results, although the simulations are a little too low at all levels. The simulated profiles are not quite symmetrical for any of the simulations.

With superficial gas velocity of 0.36 m/s, the gradient close to the wall is predicted. The magnitude of the predictions is better higher up in the riser.

For the case with superficial gas velocity of 0.71 m/s, it can be seen from figure 7, that

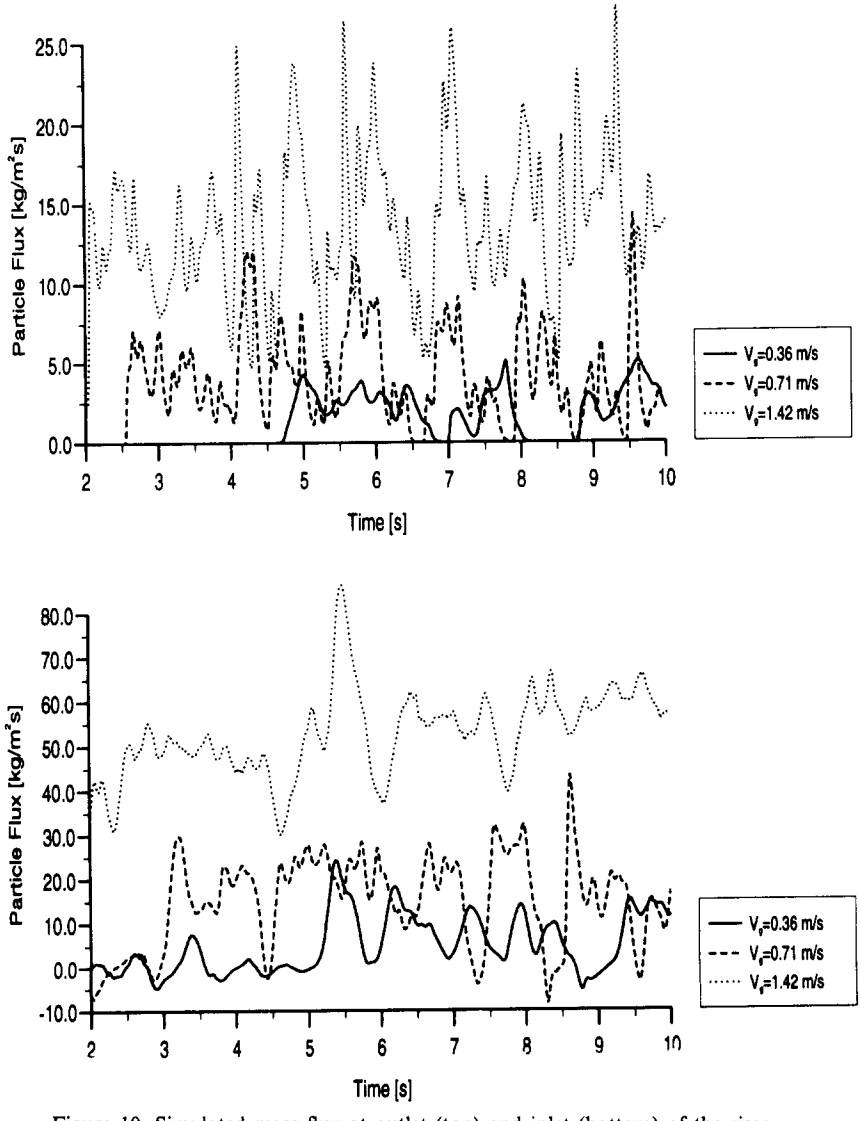

Figure 10. Simulated mass flux at outlet (top) and inlet (bottom) of the riser.

experimental RMS velocity has the steepest gradients at 0.16 m, and more evenly distributed at the higher levels. This general trend is also given by the simulations, except that the velocities are a little too low.

When the superficial gas velocity is 1.42 m/s, the simulated RMS velocity profiles have not the same general trend as the other examples had. The RMS velocity profiles have negative gradients near the walls, and that is opposite the experimental results. But the simulated results agrees well in the core where the right magnitude is predicted. The reasons for the different behaviour of the 1.42 m/s case is at present not known.

5.4. Dependence of the coefficient of restitution

The main dissipative term in the turbulent kinetic energy equation consists of the dissipation due to the particle-particle collision. This energy dissipation depends on the restitution coefficient e. Therefore, the solid shear viscosity indirectly depends on the coefficient of restitution. In this model it is considered as a constant for a given material and velocity range. Actually it depends on the velocity and it approaches unity when the impact velocity approaches zero (Meriam 1980). A handbook value for e is generally unreliable, so the value 0.995 used in the simulations is just an estimated value (Johnson 1980).

To be able to see how it will affect the granular temperature and shear viscosity, the coefficient of restitution is changed and some simulations are done with restitution coefficient of 0.9, 0.995 and 0.999. Superficial gas velocity used in these simulations is 0.71 m/s. Figure 9 shows the result for RMS velocity and shear viscosity 0.32 m above the distributor. When e equals 0.9 it is obvious that the oscillation velocity is too low, and then the shear viscosity obtain a too low value. From 0.9 to 0.995, the difference is roughly 0.25 m/s in oscillation velocity and both profiles are evenly distributed. When e changes from 0.995 to 0.999, the RMS velocity undergoes a relatively large change both in form and magnitude. The difference is roughly 1 m/s. The RMS profiles do not vary linearly with e.

The two lowest values of e gave a flat profile, whereas the highest value gave a wavy profile, and a high negative gradient close to the wall. When e equals 0.995 the velocity in the core is almost at the same level as measured, but there is no gradient near the wall. The same variations can also be seen in the profiles for shear viscosity. Gidaspow (1992) suggests that the restitution coefficient may be velocity dependent. The restitution coefficient has to decrease if the oscillation velocity increases. With e equals 0.995, the predicted viscosity is almost equal to the viscosity of liquid water at ambient temperature.

5.5. Large scale fluctuations

A fluidized system of gas and particles will never reach a steady state and a bed or a circulating reactor will exhibit a fluctuating behaviour. Figures 6–9 show the turbulent or small scale

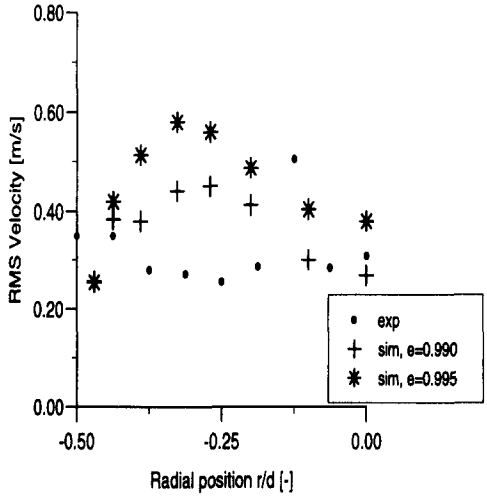

Figure 11. Experimental and simulated large and small scale RMS velocities. $V_{g,sup} = 0.36$ m/s.

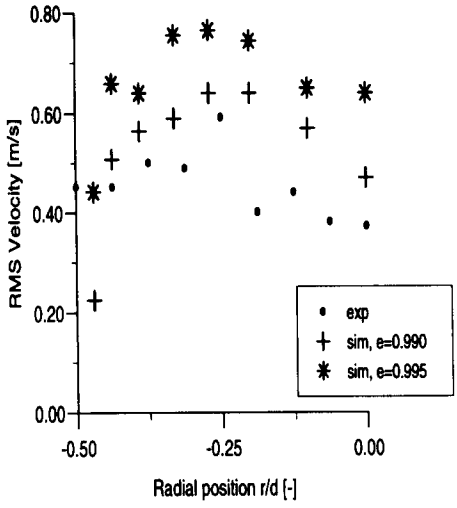

Figure 12. Experimental and simulated small and large scale RMS velocities. $V_{g,sup} = 0.71$ m/s.

fluctuations. Visually it is also easy to observe larger scale fluctuations. These large scale fluctuations are also simulated. Figure 10 shows the fluctuations of the outflowing, over the top and inflowing, from the standpipe, of the solid mass flux. For the outflowing solid mass flux, the frequency is highest for the highest gas superficial velocity. The frequency is about 1.5 Hz for the case with gas superficial velocity of 1.42 m/s, 1 Hz and 0.5 Hz for gas superficial velocity of 0.71 and 0.36 m/s, respectively. Regarding the inflowing solid mass flux, the opposite trend is shown in figure 10. The lowest gas superficial velocity has the highest frequency. The frequency is 1.2 Hz for the case with gas superficial velocity of 0.36 m/s, 0.7 Hz and 0.6 Hz for gas superficial velocity 0.71 and 1.42 m/s, respectively.

It is reason to believe that these large scale fluctuations are included in the measurements, and by that the simulated RMS velocity cannot be compared directly with the measured RMS velocity. The simulated large scale velocity fluctuations and RMS fluctuations from the simulated granular temperature can be added to give a total RMS velocity. This total RMS velocity can then be compared to the experimental RMS velocity.

Figure 11 shows the experimental and simulated RMS velocities. In the simulated results, the large and small scale fluctuations are included and the coefficient of restitution is varied from 0.990 to 0.995. The simulation shows the opposite results when compared with the measurements.

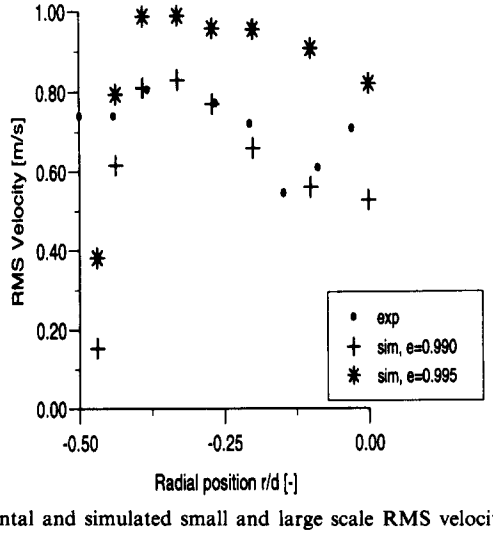

Figure 13. Experimental and simulated small and large scale RMS velocities. $V_{g,sup} = 1.42$ m/s.

In the transition range from annulus to the core, where the production of turbulence is high, the simulations have a positive gradient while the measurement has a negative gradient. The simulations gave a too high velocity in the annulus, but with restitution coefficient of 0.990, the agreement is better in the core.

For the case of gas superficial velocity of 0.71 m/s in figure 12, the trend for the predicted profile is similar in form compared to the measured profile. When e equal 0.995, a too high value is predicted whereas with e equal to 0.990 closer agreements with the measured values are found. When the gas superficial velocity is increased to 1.42 m/s, figure 13 shows that the simulation with e equals to 0.990 is almost similar to the measured values in both form and size. With e equal to 0.995, the velocity is too high compared with the measurements.

6. DISCUSSION AND CONCLUSION

A comprehensive multi-dimensional CFD model for gas particle flow has been proposed. The conservation equations for the solid phase are based on kinetic theory for dense gases, which makes it possible to calculate a granular temperature and a solid phase shear viscosity. The model is compared against experimental data from LDA measurements done in a cold flow circulating fluidized bed reactor. The general trend is in fairly good agreement with the measurements, that is, upwards flow in the core and downflow near the walls. The velocity profile and the maximum velocity in the core agreed well with the experimental data, but the downflow velocities near the walls are overpredicted. Fully developed flow is only found with the lowest superficial gas velocity, this result is supported by the measurements.

The discrepancies between the results may be due to the fact that the simulations were done with a Cartesian geometry description, whereas the actual geometry is axi-symmetric. The effect of static electricity in the experiment is unknown. Visually one could observe particles sticking to the wall and this effect may significantly reduce the downflow of particles. In addition, the assumption of an asymmetric outlet may also influence the predictions.

The turbulent kinetic energy model is capable to predict reasonable oscillations in the solid phase, but when large scale fluctuations are added, the best results are given when a lower coefficient of restitution is used. The velocity profiles and large scale velocity fluctuations are very little influenced when e is changed within the range used in the simulations, but as already seen, the RMS velocity profiles are dramatically changed. The simulated shear viscosity is near the laminar viscosity of liquid water at ambient temperature when the coefficient of restitution equals 0.995 and only based on granular temperature. There is reason to believe that large scale fluctuations must be included in the calculation of the real shear viscosity.

Acknowledgements—The present work is financially supported by Norsk Hydro a.s. and the Research Council of Norway (NFR). The authors are grateful to the following MSc students that have contributed to the work: E. Lode, H. Aadland and J. Y. Stokke.

REFERENCES

Chapman, S. & Cowling, T. G. 1970 *The Mathematical Theory of Non-uniform Gases*, 3rd edition. Cambridge University Press, Cambridge.

Deardorff, J. W. 1971 On the magnitude of the sub grid scale eddy coefficient. *J. Comp. Phys.* **7**, 120–133.

Ding, J. & Gidaspow, D. 1990 Bubbling fluidization model using kinetic theory of granular flow. *AIChE J.* **36** (4), 523–537.

Gidaspow, D. 1983 Hydrodynamics of fluidisation and heat transfer. Supercomputer modeling. *Appl. Mech. Rev.* **39** (1), 1–23.

Gidaspow, D. 1992 Multiphase flow and fluidization, continuum and kinetic theory descriptions. Lectures given at Telemark Institute of Technology and Telemark Technological R&D Centre (Tel-Tek).

Harris, B. J. & Davidson, J. F. 1993 Modelling options for circulating fluidized beds: a core/annulus deposition model. Preprint volume for the 4th Int. Conference on Circulating Fluid Beds, pp. 35–40.

Hjertager, B. H. & Samuelsberg, A. 1992 Computer simulation of flow processes in fluidized bed reactors. *KONA, Powder and Particle* **10,** 96–103.

Jenkins, J. T. & Savage, S. B. 1983 A theory for the rapid flow of identical, smooth, nearly elastic, spherical particles. *J. Fluid Mechanics* **130,** 187–202.

Johnson, K. L. 1985 *Contact Mechanics.* Cambridge University Press, Cambridge.

Lun, C. K. K., Savage, S. B., Jeffrey, D. J. & Chepurniy, N. 1984 Kinetic theories for granular flow: inelastic particles in Couette flow and slightly inelastic particles in a general flowfield. *J. Fluid Mechanics* **140,** 223–256.

Ma, D. & Ahmadi, G. 1990 A thermodynamical formulation for dispersed multiphase turbulent flows—II. *Int. J. Multiphase Flow* **16** (2), 341–351.

Meriam, J. L. 1980 *Engineering Mechanics, Vol. 2, Dynamics.* John Wiley & Sons, New York.

Sinclair, J. L. & Jackson, R. 1989 Gas-particle flow in a vertical pipe with particle–particle interactions. *AIChE J.* **35** (9), 1473–1486.

Spalding, D. B. 1985 Computer simulation of two-phase flows with special reference to nuclear reactor systems. In *Computational Techniques in Heat Transfer* (Edited by Lewis, R. W., Morgan, K., Johnsen, J. A. & Smith, W. R.), pp. 1–44. Pineridge Press, Swansea.

Tsuo, Y. P. & Gidaspow, D. 1990 Computation of flow patterns in circulating fluidized beds. *AIChE J.* **36** (6), 885–896.